Preformed Nanoporous Carbon Nanotube Scaffold-Based Multifunctional Polymer Composites

Youngseok Oh[†] and Mohammad F. Islam[*]

Department of Materials Science and Engineering, Carnegie Mellon University 5000 Forbes Avenue, Pittsburgh, Pennsylvania 15213-3815, United States
[†]Present address: Composite Research Division, Korea Institute of Materials Science, 797 Changwon-daero, Changwon, Gyeongnam 642—831, South Korea.

ABSTRACT Multifunctional polymer nanocomposites that simultaneously possess high modulus and strength, high thermal stability, novel optical responses, and high electrical and thermal conductivity have been actively researched. Carbon nanotubes are considered an ideal additive for composites because of their superlative physical, electronic and optical properties. While nanotubes have successfully added electrical conductivity, thermal stability, and novel optical responses to polymers, mechanical reinforcements, although substantial, have been well below any theoretical estimations. Here, we integrated preformed hydrogels and aerogels of individually dispersed nanotubes with polymer to increase elastic modulus of composites according to Halpin—Tsai model up to at least 25 vol % of nanotubes. Our solution-based fabrication method allowed us to create bulk composites with tunable form-factors, and with polymers that were incompatible with nanotubes. Further, in this approach, nanotubes were not covalently linked among themselves and to the polymer, so intrinsic optical, electrical, and thermal properties of nanotubes could be exploited. The optically active nanotubes, for example, added a strain-dependent, spatially resolved fluorescence to these composites. Finally, the nanoporous nanotube networks suppressed the polymer glass transition and extended the mechanical integrity of polymer well above its polymer melting point, and both the nanotubes and polymer remained thermally stable above their decomposition temperatures.

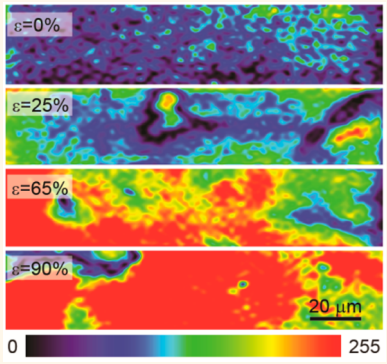

KEYWORDS: multifunctional nanocomposites · modulus · carbon nanotubes · aerogels

Multifunctional polymer composites that simultaneously possess high modulus and strength, high thermal stability, novel optical responses, and high electrical and thermal conductivity have been extensively researched over the last several decades.[1,2] Carbon nanotubes combine low density (~1.3 g/mL), large aspect ratio (typically ≥1000), and high surface area per mass and volume (~1315 m^2/g and ~10^9 m^2/m^3, respectively) with exceptional mechanical (elastic modulus, $E \approx$ 1 TPa and ultimate tensile strength, UTS ≈ 200 GPa), electrical, thermal and optical properties,[3—5] which should make them an ideal additive to impart these multifunctionalities to polymers. Thus far, nanotubes separately added thermal stability,[6] electrical conductivity,[7,8] and fluorescence[9] to polymer composites. However, nanotube induced mechanical property enhancements of composites, although substantial,[10—20] had been significantly below estimates based on the rule of mixtures, the Mori—Tanaka or the Halpin—Tsai models.[11,21] Further, concurrent incorporations of all of these functionalities to composites have not been achieved.

Mechanical reinforcements of polymers by nanotubes, which already possess high stiffness along with a large aspect ratio and surface area per volume, require them to be homogeneously dispersed at high volume fraction within the polymer matrix and have strong interfacial adhesion with polymers to promote effective load transfer from the polymer to the nanotubes.[11,22,23] Unfortunately, nanotubes aggregate when simply mixed with polymers: van der Waals attraction between nanotubes is stronger than nanotube adhesion to polymers. As a result, direct dispersion of 1—20 vol % of nanotubes of lengths between hundreds of nanometers and tens of micrometers into polymers,[10—17] the most widely used fabrication method, led to mechanical enhancements

* Address correspondence to mohammad@cmu.edu.

Received for review January 9, 2015 and accepted March 19, 2015.

Published online March 20, 2015
10.1021/acsnano.5b00170

that were significantly below any model-based estimations.[11,21] This insufficient reinforcement had also been attributed to short nanotube lengths as well as bundling and slippage of nanotubes at their atomically smooth surfaces.

Covalent functionalization of nanotubes reduced nanotube aggregation and allowed chemical cross-linking of nanotubes to polymers, which in turn enhanced interfacial adhesion with polymers.[18,19] These chemically functionalized nanotubes had also been cross-linked among themselves to form networks that had then been backfilled with polymers to create composites.[19] Chemical cross-linking between polymers and nanofillers typically increased E of the composites by ~10-fold compared to their un-cross-linked counterpart.[20] However, this approach destroyed intrinsic properties of nanotubes, and the mechanical reinforcements were either not observed[19] or were still well below theoretical estimates.[18] To achieve homogeneous nanotube dispersion in polymers without covalent functionalization, preformed porous networks of ultralong nanotubes of hundreds of micrometers to centimeters had been backfilled with polymers.[8,12−15] These porous nanotube networks were typically fabricated *via* chemical vapor deposition method, and they contained impurities from synthesis that could not be removed without destroying the network. Further, they offered limited control over porosity, form-factor and properties of the constituent nanotubes. Backfilling of these networks, which had 1.5−60 vol % nanotubes, had yielded enhancements in E and UTS that were far below estimates,[12−15] possibly because nanotubes bundled during synthesis and/or polymer infiltration, and had poor interfacial adhesion with polymers.

Herein, we demonstrate an increase in E of the composites according to Halpin−Tsai model up to at least 25 vol % of nanotube loading by backfilling preformed hydrogels or aerogels of individually dispersed single-walled carbon nanotubes (SWCNTs) with polymer without covalently linking the nanotubes to each other and to the polymer. Our solution-based fabrication method also allowed us to use purified, property-selected nanotubes to create bulk composites with tunable form-factors, and with polymers that were incompatible with nanotubes. Furthermore, in this approach, nanotubes were not covalently linked among themselves and to the polymer so the intrinsic optical, electrical and thermal properties of nanotubes could be exploited. For example, the optically active nanotubes added a strain-dependent, spatially resolved fluorescence to these composites. Finally, the nanoporous nanotube networks suppressed the polymer glass transition and extended the mechanical integrity of polymer well above its polymer melting point, and both the nanotubes and polymer remained thermally stable above their decomposition temperatures.

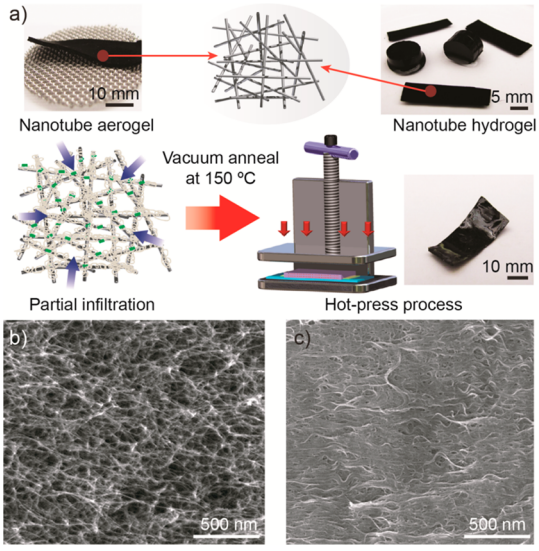

Figure 1. Nanotube hydrogel- and aerogel-based polymer composites. (a) A schematic of the fabrication steps. (b) Scanning electron microscopy imaging of a cross section of nanotube aerogels of 0.8 vol % showed three-dimensional network of isolated nanotubes. (c) Similar imaging of composites with 25 vol % nanotubes showed that the nanotube networks were unaffected by polymer infiltration, and the composites did not have any voids. More images are shown in Supporting Information Figure S1e,f.

RESULTS AND DISCUSSION

A schematic representation of our composite fabrication method is shown in Figure 1a. We used a new class of networks of short, purified and solution processed[4,5,24] SWCNTs of average length ≈1 μm in hydrogel- and aerogel-forms[25−29] of concentration 0.8 vol % as preformed scaffolds for composite fabrication. The network was held together primarily *via* van der Waals interactions at discrete nanotube cross-linking points or "nodes".[26,27] The nanotubes within these scaffolds were individually dispersed and randomly oriented, as captured in high-resolution scanning and transmission electron microscopy (HR-SEM and HR-TEM, respectively) images of their cross sections (Figure 1b and Supporting Information Figure S1a). These scaffolds possessed pores of diameters 4−28 nm,[29] which were suitable for easy infiltration of polymers, and very large surface area per mass (Brunauer−Emmett−Teller surface area ~1291 m^2/g) and per volume (~10^7 m^2/m^3),[29] which were essential for effective load transfer from polymers to nanotubes.[30] The polymer we used was thermoplastic polyurethane (TPU), which is a random block copolymer of hard and soft segments (HS and SS, respectively). This class of polymers is often utilized as a matrix in nanocomposite studies since it has wide industrial applications, versatile chemical synthesis routes, and easy processing. To prepare composites, we first exchanged water and air in nanotube hydrogels and aerogels, respectively, with an appropriate solvent such as tetrahydrofuran (THF) that also dissolved the

polymer; we hereafter refer to these THF-filled nanotube scaffolds as wetgels. We partially backfilled these wetgels with polymer by soaking them in polymer solutions of concentrations 3−10 wt % in THF for 6−12 h at 50 °C. By adjusting the polymer solution concentration and soaking time, we varied the final nanotube vol % in the composites. At the backfilling temperature, the polymer was in a rubbery state, and the viscosities of the polymer solutions were low, which facilitated easy infiltration. We then evaporated the solvent, annealed the composites under vacuum at 150 °C for 10 h, and removed all voids by hot-pressing the composites at 130 °C for 5 min; the two latter steps did not induce fracturing of the composites since the polymer was in a melted state. The partially polymer-filled nanotube scaffolds did not show any appreciable volume shrinkage during solvent evaporation step, but the annealing step caused 5−10% volume shrinkage that depended on the polymer content within the scaffold. The composites used for all measurements were rectangular with an average thickness of 200 μm (Figure 1) and had a void volume fraction $\leq$0.0013%. HR-SEM imaging of a cross section of the composites showed that the nanotube networks were well preserved after the fabrication process with no discernible voids (Figure 1c and Supporting Information Figure S1e,f). HR-TEM images showed that the polymer coated the nanotubes including the nodes (Supporting Information Figure S1b−d) that likely allowed densification under hot-press without a disintegration of the network or bundling of nanotubes. Furthermore, the substantial polymer coating of the nanotubes probably also hindered noticeable alignment of nanotubes normal to or along hot-press direction (Figure 1c and Supporting Information Figure S1e,f).

To assess the mechanical reinforcement of polymer by the nanotube networks, we compared mechanical characteristics of the composites with up to 25 vol % nanotubes to that of nanotube scaffolds and polymer from measurements of tensile stress (σ) *versus* tensile strain (ε) at room temperature (Figure 2a). For nanotube scaffolds, we measured mechanical properties in compression because our previous work demonstrated that elastic moduli from compressive and tensile measurements were nearly identical due to the random orientation of nanotubes,[29] and the grips that hold samples in the tensile instrument often cracked nanotube scaffolds. The compressive stress increased linearly with compressive strain until ~9% for all nanotube aerogel-based scaffolds and the compressive elastic moduli increased from 0.21 MPa at 0.8 vol % to 21.5 MPa at 25 vol % nanotubes (Supporting Information Figure S2). Nanotube hydrogel-based scaffolds showed similar mechanical characteristics but had ~10× lower elastic moduli at the same concentration.[27] The polymer showed linear deformation for $\varepsilon \leq$ 10% with E of 6.63 MPa (Figure 2a), then

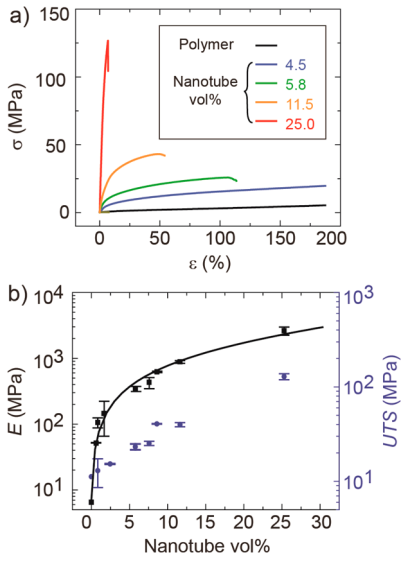

Figure 2. Mechanical characteristics of composites. (a) The tensile stress (σ) *versus* tensile strain (ε) curves of polymer and composites with various nanotube concentrations. (b) The tensile moduli (E) of the composites (black solid symbols) increased by >40 000% with an addition of 25 vol % of nanotubes. The measured E of the composites was well predicted by the Halpin−Tsai model (black solid line). The ultimate tensile strength (UTS) of the composites (blue solid symbols) also increased with the addition of nanotubes. The error bars were obtained from measurements on multiple samples.

plastically yielded to a more gradual deformation followed by a steep rise in σ up to a stretchability of ~400% at which point the specimen broke. E of the composites increased dramatically with nanotube addition and reached 2688.5 MPa at 25 vol % nanotube (Figure 2b), which corresponds to >40 000% improvements over that of the polymer. However, the yield point began at smaller strain and stretchability decreased with an increase in nanotube concentration. Composites prepared from hydrogel-based scaffolds had larger stretchability but slightly lower specific enhancement in moduli, *i.e.*, enhancement per nanotube volume fraction $(E_c - E_m)/(E_m V_f)$, where E_c and E_m are the tensile moduli of the composites and the polymer, respectively, and V_f is the nanotube volume fraction, compared to aerogel-based scaffolds with similar nanotube loading. Most of the measurements are from composites that were fabricated from hydrogel-based scaffolds.

The yield strength (σ_y) and the modulus of resilience of the composites (U_r) also showed profound improvements. σ_y of composites reaches 50.1 MPa with 25 vol % of nanotubes which represents >13 800% improvement over that of the polymer which was 0.36 MPa (Figure 3a). Note that the composites did not show any sudden drop in σ_y after yield, which has been commonly observed for other TPU-based nanocomposites due to disintegration of percolating nanofiller network,[31] and this demonstrates the robustness of the nanotube scaffolds within the composites. U_r increased by

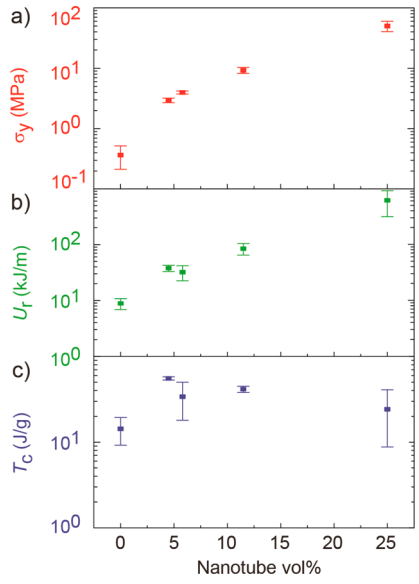

Figure 3. Yield strength (σ_y), the modulus of resilience (U_r) and the toughness (T_c) of the composites. (a) σ_y and (b) U_r dramatically increased with an increase in nanotube concentration. (c) In contrast, T_c of the composites increased up to an addition of 4.5 vol % nanotubes but then gradually decreased with an increase in nanotube concentration.

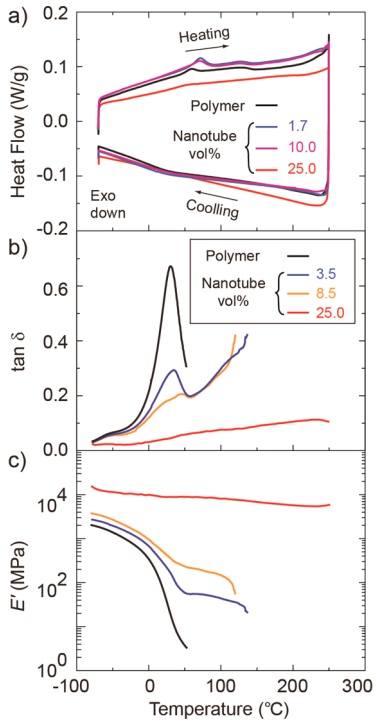

Figure 4. Thermomechanical characteristics of composites. (a) Differential scanning calorimetry measurements of polymer and composites showed reduction in polymer crystallization in the composites with increasing nanotube concentration. (b) Damping ratio (tan δ) *versus* temperature also showed a reduction in glass transition of the hard segments. (c) The storage moduli (E') *versus* temperature measurements showed that the nanotube networks extended mechanical integrity of composites well beyond the polymer melting temperature (~58.9 °C).

~6897% from 8.83 kJ/m^3 for polymer to 617.82 kJ/m^3 for composites with 25 vol % nanotubes (Figure 3b). Further, these nanotube composites showed enhancement in UTS from 11.43 MPa for polymer to 125.4 MPa (~1000%) at the highest nanotube vol % (Figure 2b). Interestingly, the toughness (T_c) of the composites increased by ~300% at 4.5 vol % nanotubes, then gradually decreased with further increase in nanotube concentration (Figure 3c), indicating an optimal nanotube loading for toughness enhancement. Note, the T_c of composites with 4.5 vol % nanotubes (~50.8 J/g) was larger than that of Kevlar fiber (25−33 J/g).[14] The specific enhancements in E and UTS we report here (~1618 and ~40, respectively) are few times to an order of magnitude larger than the reported reinforcements from composites of the same polymer and SWCNTs (~6 and ~28, respectively),[32] multiwalled carbon nanotubes (~28 and ~8, respectively),[33] and nanoclays (~108 and ~5, respectively).[31]

To elucidate the origin of the mechanical enhancement, we investigated nanotube network-induced changes in polymer morphology. We examined polymer crystallinity and effective stiffness, both of which typically enhance E but also reduce T_c,[11] using differential scanning calorimetry (DSC) analysis, X-ray diffraction (XRD) and dynamic mechanical analysis (DMA). For polymer, the DSC curve from the first heating, *i.e.*, endotherm, cycle showed a small peak at ~58.9 °C. This peak indicated that the hard segments formed weakly crystalline domains that melted at this temperature ($T_{m,HS}$) with an absorbed heat ΔH_m of 3.4 J/g, calculated from the area under the peak, while the soft segments showed no crystallinity (Figure 4a). The melting of the hard segments was reversible and showed a much weaker recrystallization on cooling, *i.e.*, exotherm, cycle at ~30 °C after previous thermal history was erased in the endotherm cycle. The glass transitions of both the hard and soft segments were too broad to precisely determine the transition temperatures $T_{g,HS}$ and $T_{g,SS}$ from the DSC curve and were instead determined from the DMA measurements. Further, the DSC analysis on an extended temperature range showed that the soft and hard segments decomposed around 325 and 400 °C, respectively (Supporting Information Figure S3). ΔH_m, and thus polymer crystallinity, initially remained nearly unchanged up to ~10 vol % of nanotube addition, but $T_{m,HS}$ shifted to a higher temperature (~70 °C). With a further increase in nanotube concentration, the intensity of the endotherm peak decreased and eventually became barely discernible for composites with 25 vol % nanotubes. This decrease suggested reduced crystallinity of the hard segments, possibly due to their restricted thermal motion within the nanoporous nanotube networks.[16,31,34,35] We confirmed the decreased polymer crystallinity in the presence of the nanotube network by XRD measurements (Supporting Information Figure S4). The peak location in the XRD patterns was

unaffected by the nanotube addition, which indicated that the crystalline domain sizes did not change with nanotube loading. DSC curves also indicated that the nanotube network shifted the decomposition temperature of the hard segments to a higher temperature (~450 °C) while the decomposition temperature for soft segments remained nearly unaltered (Supporting Information Figure S3). This higher decomposition temperature extended mechanical integrity and thermal stability of the polymer, discussed below.

The nanotube-induced constrained thermal motion of the polymer was also revealed through the altered glass transition and melting behavior of the polymer. We determined $T_{g,SS}$ and $T_{g,HS}$ from the viscoelastic properties measured by DMA (Figure 4b). Note, nanotube networks did not show any glass transition over the experimental frequency and temperature range.[26−29] For polymer, $T_{g,SS}$ and $T_{g,HS}$ appeared ~−50 °C and ~30 °C, respectively. With the addition of nanotube networks, the amplitude of the glass transition peaks for the soft and the hard segments decreased , but $T_{g,SS}$ remained nearly the same while $T_{g,HS}$ shifted to higher temperature. For composites with 25 vol % of nanotubes, $T_{g,SS}$ and $T_{g,HS}$ were not readily identifiable until mechanical failure of the specimens at 250 °C, which suggested that the glass transitions of both segments were either broad or nearly suppressed. Further, the storage modulus E' increased dramatically in the presence of the nanotube network, especially above $T_{g,SS}$ (Figure 4c). E' at room temperature for polymer and composites were comparable to E measured from the tensile test (Figure 2b). The polymer specimens fractured at ~50 °C, likely due to the melting of the soft segments, whereas the mechanical failure of the composites was shifted to a higher temperature with an increase in nanotube loading. Composites with 25 vol % nanotubes showed almost no degradation in E' until the specimen broke at 250 °C, which suggested that the nanotube network acted as a rebar to provide additional mechanical integrity to polymer over an extended temperature range beyond the polymer melting temperature (~58.9 °C). The restrained polymer thermal motion, which could be thought of as an increase in the effective polymer stiffness, likely had contributed to the observed mechanical reinforcement.

There is no comprehensive theory that combines reinforcements from a three-dimensional percolating network with accentuated polymer stiffness from confinement.[18,20,31,34,35] To estimate E_c, we employed Halpin−Tsai equation for composites reinforced with randomly oriented short fibers, *i.e.*, fibers that did not span the entire length of the composite specimen),[11] which had been successfully applied to nanotube based composites:[11,14] $E_c = (3/8)E_{11} + (5/8)E_{22}$, where $E_{11} = E_m(1 + \zeta\,\eta_L V_f)/(1 - \eta_L V_f)$ was the longitudinal modulus and $E_{22} = E_m\,(1 + 2\,\eta_T V_f)/(1 - \eta_T V_f)$ was the transverse modulus. In this expression, ζ was $2l/D = 2000$ where average nanotube length $l \approx 1000$ nm and diameter $D \approx 1$ nm as per manufacturer (Southwest Nanotechnology) specification, $\eta_L = (E_f/E_m - 1)/(E_f/E_m + \zeta)$, $\eta_T = (E_f/E_m - 1)/(E_f/E_m + 2)$ and E_f was the tensile modulus of nanotubes ~1 TPa[3]). In this form, the expression did not have any free parameters. The calculated E_c at various nanotube loadings (black solid line in Figure 2b) showed excellent agreement with the experimentally measured E_c (black solid symbols in Figure 2b). Note, E_f used in the estimation was at the low end of the tensile modulus of SWCNTs and use of a modulus at the higher end (*e.g.*, 1.4 TPa[3]) did not degrade the quality of the agreement. Similarly, varying the aspect ratio $\zeta/2$ from 1000 to 800 or 1200 introduced negligible changes to the estimation of E_c. Nevertheless, we fabricated composites with 3 vol % of HiPCO type SWCNTs with a narrow length distribution (150 ± 17 nm),[36] and the measured E_c agreed well with estimation based on Halpin−Tsai equation. We also recognize that the Halpin−Tsai equation assumes perfect interfacial adhesion between nanotubes and polymer, which is unlikely to be true here because nanotubes were not covalently linked to polymer and had highly smooth surfaces. Indeed, we estimated the interfacial shear stress from measured UTS to be quite low (~0.46 MPa, see Supporting Information Figure S5). Similar low interfacial shear stress was estimated from strain dependent Raman shifts of the 2D band of SWCNTs[3] (~0.64 MPa, see Supporting Information Figure S6). However, since the nanotubes had an aspect ratio ≫10, the correction to E_{11} from low interfacial shear stress was likely to be small.[11] We attribute the exceptional mechanical reinforcement by nanotubes and the excellent agreement with Halpin−Tsai equation based estimation, despite low interfacial shear stress, to efficient load transfer from the polymer to nanotubes brought about by polymer hindering the sliding of nanotubes at the nodes coupled with the ultrahigh surface area per volume of nanotube hydrogels and aerogels (>10^7 m^2/m^3).

The intrinsic properties of individually dispersed, undamaged nanotubes also added several other beneficial features to the composites. For example, these composites were highly electrically conducting (Supporting Information Figure S7), although aerogel-based composites were more conducting than hydrogel-based composites, possibly because polymer penetrated the nodes and degraded the electrical contact between nanotubes. All composites also showed extended thermal stability and a slower mass loss rate when burned in atmospheric air in thermogravimetric analysis (Supporting Information Figure S8a,b),[6] likely from the shift in decomposition temperature of the hard segments to a higher temperature (see DSC measurements in Methods and Supporting Information Figure S3). The nanotube network remained intact

even after the composites were heated to 800 °C (Supporting Information Figure S8c and the inset) but had a thin coating of residues, probably decomposed polymer. Further, these residual nanotubes showed negligible disorder as can be seen in the Raman spectra (Supporting Information Figure S8d), even though nanotubes typically disintegrate over 400−550 °C (Supporting Information Figures S9a,b).

One of the striking features of these composites was their strain dependent fluorescence in the near-infrared region arising from the intrinsic optical properties of nanotubes.[3,4] Since individually dispersed nanotubes?> fluoresce in the near-infrared, it was reasonable to expect fluorescence from these composites. However, without any external strain, nanotubes were in contact with each other at the nodes within the composites, which likely quenched the fluorescence. As such, the composites showed almost no fluorescence except (6,5) peak near 990 nm without any external tensile stretch (Supporting Information Figure S9). As the composites were stretched, nanotubes within the composites began to get pulled away from one another, which decreased fluorescence quenching (Supporting Information Figure S9), and led to an increase in the amplitude of the fluorescence intensity of the (6,5) peak. Furthermore, the composites also started to emit broad fluorescence from (8,3) peak around 970 nm. The average separation between the nanotubes increased with an increase in tensile strain, and thus the composites exhibited a strain dependent increase in fluorescence intensity. Further, a two-dimensional mapping of the fluorescence intensity using optical microscopy also showed the spatial distribution of intensity including identification of high and low strain regions within the specimen (Figure 5). Note, since the interfacial stress between the polymer and the nanotubes was low and since we did not observe any Raman shift in the 2D band of SWCNTs (Supporting Information Figures S5 and S6), we suggest that the strain dependent changes in fluorescence intensity were not due to strain on nanotubes but rather due to a decrease in fluorescence quenching arising from a reduction in contacts between nanotube at the nodes.

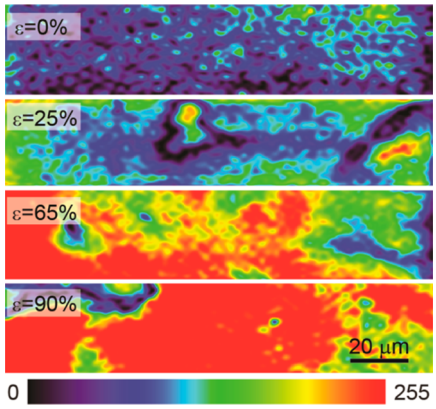

Figure 5. Spatially resolved, two-dimensional map of fluorescence response in the near-infrared region from a composite with 4.5 vol % nanotubes at four different strains. Color scale is shown below the image. The average fluorescence intensities from this composite at different strains are shown in Supporting Information Figure S9.

CONCLUSIONS

We integrated preformed hydrogels and aerogels of individually dispersed nanotubes with polymer to increase elastic modulus of composites according to Halpin−Tsai model up to at least 25 vol % of nanotube loadings without covalently liking the nanotubes to each other and to the polymer. The nanotubes also increased strength and toughness of the polymer, and added electrical conductivity and strain-dependent optical responses to the composites. The nanopores of the nanotube network reduced polymer thermal motion, resulting in a suppression of polymer glass transition and an extension of mechanical integrity above the polymer melting point. Further, the nanotubes and polymer were thermally stable well above their decomposition temperatures. Our solution-based fabrication method did not depend on the polymer type, and is similar to current methods used in industry, making our approach suitable for rapid implementation.

METHODS

Polymer Characteristics. Thermoplastic polyurethane (TPU) is a commercial grade elastomeric random block copolymer (commercial trade name Texin Sun-3006HF), and was obtained from Bayer Materials. The soft segments composed of poly(tetramethylene ether)glycol of molecular weight 1000 g/mol. The hard segments were a mixture of 4,4′-methylene diphenyl diisocyanate and 1,4-butanediol. The weight ratio between hard and soft segments was 38:62. The aliphatic hard segments of TPU were incompatible with soft segments and phase segregated into amorphous or crystalline domains within a network of soft segments. The composition and the hierarchial structures formed by both soft and hard segments dictated the thermomechanical responses of TPU: the hard segments typically influenced the modulus and strength while the soft segments provided the stretchability. The hard segments formed small crystallized domains that melted at a temperature $T_{m,HS} \sim 58.9$ °C (Figure 4a). Further, the glass transition temperature of the hard segments was $T_{g,HS} \approx 30$ °C and the soft segments were rubbery at room temperature with a $T_{g,SS} \approx -50$ °C (Figure 4b). The $T_{m,HS} \sim 58.9$ °C (Figure 4a).

Nanotube Characteristics. We used purified CoMoCAT SWCNTs to prepare nanotube hydrogels, aerogels and wetgels. The nanotubes were purchased from SouthWest NanoTechnologies, Inc. (batch CG100) and had diameters ≈1 nm, lengths ≈1 μm resulting in an aspect ratio ≈1000. The SWCNTs were purified and individually suspended in water using sodium dodecylbenzenesulfonate (SDBS) surfactant (Acros Organics).[5,24,37] The dispersed nanotubes were shaped into hydrogels and aerogels according to methods previously reported.[26−29] Energy-dispersive X-ray spectroscopy measurements on similarly produced gels showed that our fabrication process essentially removed all surfactants from the nanotube gels.[29]

To prepare composites, we exchanged water and air in hydrogels and aerogels, respectively, with THF. We chose THF because it also dissolves the polymer; we refer to THF-filled hydrogels and aerogels as wetgels.

Void Volume Fraction, V_p. We calculated V_p using the expression: $V_p = 1 - (V_f + V_m)$, where $V_f = (W_f\rho_m)/[W_f\rho_m + (1 - W_f)\rho_f]$ was the nanotube volume fraction and V_m was the polymer volume fraction.[38] In this expression, ρ_f was the density of nanotubes (1.3 g/mL), ρ_m was the density of polymer (1.08 g/L; material product sheet), and W_f was the weight fraction of nanotubes.

Microstructure Characterization. The porous three-dimensional networks of nanotubes within the aerogels and composites were imaged using scanning and transmission electron microscopy. We used an FEI Quanta 600 to obtain high resolution scanning electron microscope (HR-SEM) images and a JEOL 2100F at 75 kV to collect high resolution transmission electron microscope (HR-TEM) images.

Mechanical Characterization. The tensile stress (σ) was measured as a function of tensile strain (ε) at a rate of 0.15 mm/s at room temperature with a 50 N load cell using an Instron 5940 series tabletop testing system (TA Instruments). The instrument had a position control resolution of <0.1 μm and could measure position with an accuracy of 0.1% of displacement. For the tensile measurements, we followed the ASTM standard ASTM D 882 including the testing of plastic sheets with the thickness less than 0.25 mm. For stress *versus* strain measurements in compression loading of nanotube aerogels, we used the same instrument and settings but with compression heads. Cylindrical aerogel samples were loaded between the two compression heads with the top head applying uniaxial compression on the sample along the vertical direction. We also applied ~5% prestrain to make a uniform flat contact between the compression heads and the sample and to prevent slipping of the sample.

Thermomechanical Characterization. We measured the storage modulus (E'), loss modulus (E'') and the damping ratio (tan δ), which is E''/E', of the polymer and the composites as a function of temperature from −80 to 250 °C using a RSA-G2 DMA instrument (TA Instruments). Rectangular samples were loaded between two tension heads with a constant axial force of 0.5 N, which corresponded to ~0.5% prestrain, and with the top head oscillating along the vertical direction to apply uniaxial tension at a fixed frequency of 1 Hz and an oscillatory strain of ±1%. $T_{g,SS}$ and $T_{g,HS}$ were determined from the peak locations in plots of tan δ *versus* temperature.

Differential Scanning Calorimetry Analysis. DSC measurements were carried out with a Q20 DSC (TA Instruments) at a heating rate of 3 °C/min. Most of the measurements were collected over a temperature range of −60 to 250 °C. Polymer and composites with 10 vol % nanotubes were also tested over a temperature range of −60 to 500 °C. TGA measurements was carried out under atmospheric air over a temperature range of 25 to 800 °C using a Q50 TGA (TA Instruments). The specimens were heated at a rate of 5 °C/min.

Raman Spectroscopy and near-Infrared Fluorescence Imaging Microscopy. The Raman spectra and near-infrared fluorescence images were collected using an inverted Raman confocal microscope (inVia Raman microscope, Renishaw) with a 20× (0.40 NA) objective (Leica Microsystems) and a 785 nm (1.58 eV) laser line. For both spectra and image collections, laser power was set to 10 mW to avoid heat-induced damage to the samples. The laser spot size was 1−2 μm with an exposure time of 3 s. For Raman spectroscopy, we collected 10 scans each at five different locations for each sample and averaged the scans to improve signal-to-noise ratio. The near-infrared fluorescence images were collected in a rectangular grid with step sizes of ≤2.0 μm. The parameters for Raman spectra collection and the two-dimensional fluorescence mapping as well as all subsequent data analysis were performed using WiRE software (Renishaw). Each Raman spectrum and fluorescence intensity was then normalized by its G-band, which is a characteristics Raman signature of carbon nanotubes, intensity.

Electrical Characterization. For electrical conductivity measurements of the composites, copper wire leads were attached to the short ends of the rectangular composites with silver paste (DuPont 4929N) and resistance was measured using two-probe contact direct current method with EC-Lab V10 and Fluke Ohmmeter.

Conflict of Interest: The authors declare no competing financial interest.

Supporting Information Available: Supporting figures: (1) high resolution transmission and scanning electron microscopy images of cross sections of nanotube aerogels and polymer composites; (2) compressive stress *versus* compressive strain of aerogels with 0.8 and 25 vol % nanotubes; (3) differential scanning calorimetry analysis of polymer and composite with 10 vol % nanotubes over a wider temperature range of −60 to 500 °C; (4) the X-ray diffraction measurements of polymer and composites; (5) the determination of the interfacial shear stress between the polymer and the nanotubes from the experimentally measured ultimate tensile strength of the composites with various nanotube loadings; (6) estimation of the interfacial shear stress between the polymer and the nanotubes from tensile strain dependent Raman shifts of the 2D band of SWCNTs; (7) electrical conductivity of composites as a function of nanotube vol %; (8) thermal stability of the nanotubes and the composites; and (9) the average fluorescence intensity in the near-infrared region from the composites with 4.5 vol % nanotubes as a function of tensile strain. This material is available free of charge *via* the Internet at http://pubs.acs.org.

Acknowledgment. We acknowledge Bayer Materials for providing thermoplastic polyurethane. This work was supported by the National Science Foundation through grant CMMI-1335417. M.F.I. developed and designed the project. Y.O. carried out experiments as well as collected and analyzed data. M.F.I. gave technical and conceptual advice. Y.O. and M.F.I. wrote the manuscript and have given approval to the final version of the manuscript.

REFERENCES AND NOTES

1. Ajayan, P. M.; Tour, J. M. Materials Science—Nanotube Composites. *Nature* **2007**, *447*, 1066–1068.
2. Winey, K. I.; Vaia, R. A. Polymer Nanocomposites. *MRS Bull.* **2007**, *32*, 314–322.
3. Dresselhaus, M. S.; Dresselhaus, G.; Avouris, P. *Carbon Nanotubes: Synthesis, Structure, Properties, and Applications*; Springer: Berlin, 2001.
4. Islam, M. F.; Milkie, D. E.; Kane, C. L.; Yodh, A. G.; Kikkawa, J. M. Direct Measurement of the Polarized Optical Absorption Cross Section of Single-Wall Carbon Nanotubes. *Phys. Rev. Lett.* **2004**, *93*, 037404.
5. Johnston, D. E.; Islam, M. F.; Yodh, A. G.; Johnson, A. T. Electronic Devices Based on Purified Carbon Nanotubes Grown by High-Pressure Decomposition of Carbon Monoxide. *Nat. Mater.* **2005**, *4*, 589–592.
6. Kashiwagi, T.; Du, F.; Douglas, J. F.; Winey, K. I.; Harris, R. H., Jr.; Shields, J. R. Nanoparticle Networks Reduce the Flammability of Polymer Nanocomposites. *Nat. Mater.* **2005**, *4*, 928–933.
7. Bryning, M. B.; Islam, M. F.; Kikkawa, J. M.; Yodh, A. G. Very Low Conductivity Threshold in Bulk Isotropic Single-Walled Carbon Nanotube-Epoxy Composites. *Adv. Mater.* **2005**, *17*, 1186–1191.
8. Gui, X. C.; Li, H. B.; Zhang, L. H.; Jia, Y.; Liu, L.; Li, Z.; Wei, J. Q.; Wang, K. L.; Zhu, H. W.; Tang, Z. K.; et al. A Facile Route to Isotropic Conductive Nanocomposites by Direct Polymer Infiltration of Carbon Nanotube Sponges. *ACS Nano* **2011**, *5*, 4276–4283.
9. Graff, R. A.; Swanson, J. P.; Barone, P. W.; Baik, S.; Heller, D. A.; Strano, M. S. Achieving Individual-Nanotube Dispersion at High Loading in Single-Walled Carbon Nanotube Composites. *Adv. Mater.* **2005**, *17*, 980.
10. Vigolo, B.; Pénicaud, A.; Coulon, C.; Sauder, C.; Pailler, R.; Journet, C.; Bernier, P.; Poulin, P. Macroscopic Fibers and Ribbons of Oriented Carbon Nanotubes. *Science* **2000**, *290*, 1331–1334.

11. Coleman, J. N.; Khan, U.; Blau, W. J.; Gun'ko, Y. K. Small but Strong: A Review of the Mechanical Properties of Carbon Nanotube-Polymer Composites. *Carbon* **2006**, *44*, 1624–1652.
12. Kobashi, K.; Nishino, H.; Yamada, T.; Futaba, D. N.; Yumura, M.; Hata, K. Epoxy Composite Sheets with a Large Interfacial Area from a High Surface Area-Supplying Single-Walled Carbon Nanotube Scaffold Filler. *Carbon* **2011**, *49*, 5090–5098.
13. Ci, L.; Suhr, J.; Pushparaj, V.; Zhang, X.; Ajayan, P. M. Continuous Carbon Nanotube Reinforced Composites. *Nano Lett.* **2008**, *8*, 2762–2766.
14. Ma, W. J.; Liu, L. Q.; Zhang, Z.; Yang, R.; Liu, G.; Zhang, T. H.; An, X. F.; Yi, X. S.; Ren, Y.; Niu, Z. Q.; et al. High-Strength Composite Fibers: Realizing True Potential of Carbon Nanotubes in Polymer Matrix through Continuous Reticulate Architecture and Molecular Level Couplings. *Nano Lett.* **2009**, *9*, 2855–2861.
15. Zeng, Y.; Ci, L. J.; Carey, B. J.; Vajtai, R.; Ajayan, P. M. Design and Reinforcement: Vertically Aligned Carbon Nanotube-Based Sandwich Composites. *ACS Nano* **2010**, *4*, 6798–6804.
16. Miaudet, P.; Derré, A.; Maugey, M.; Zakri, C.; Piccione, P. M.; Inoubli, R.; Poulin, P. Shape and Temperature Memory of Nanocomposites with Broadened Glass Transition. *Science* **2007**, *318*, 1294–1296.
17. Cheng, Q. F.; Bao, J. W.; Park, J.; Liang, Z. Y.; Zhang, C.; Wang, B. High Mechanical Performance Composite Conductor: Multi-Walled Carbon Nanotube Sheet/Bismaleimide Nanocomposites. *Adv. Funct. Mater.* **2009**, *19*, 3219.
18. Shim, B. S.; Zhu, J.; Jan, E.; Critchley, K.; Ho, S.; Podsiadlo, P.; Sun, K.; Kotov, N. A. Multiparameter Structural Optimization of Single-Walled Carbon Nanotube Composites: Toward Record Strength, Stiffness, and Toughness. *ACS Nano* **2009**, *3*, 1711–1722.
19. Capadona, J. R.; Van Den Berg, O.; Capadona, L. A.; Schroeter, M.; Rowan, S. J.; Tyler, D. J.; Weder, C. A Versatile Approach for the Processing of Polymer Nanocomposites with Self-Assembled Nanofibre Templates. *Nat. Nanotechnol.* **2007**, *2*, 765–769.
20. Podsiadlo, P.; Kaushik, A. K.; Arruda, E. M.; Waas, A. M.; Shim, B. S.; Xu, J. D.; Nandivada, H.; Pumplin, B. G.; Lahann, J.; Ramamoorthy, A.; et al. Ultrastrong and Stiff Layered Polymer Nanocomposites. *Science* **2007**, *318*, 80–83.
21. Halpin, J. C.; Kardos, J. L. The Halpin-Tsai Equations: A Review. *Polym. Eng. Sci.* **1976**, *16*, 344–352.
22. Nie, Z.; Fava, D.; Kumacheva, E.; Zou, S.; Walker, G. C.; Rubinstein, M. Self-Assembly of Metal–Polymer Analogues of Amphiphilic Triblock Copolymers. *Nat. Mater.* **2007**, *6*, 609–614.
23. Akcora, P.; Liu, H.; Kumar, S. K.; Moll, J.; Li, Y.; Benicewicz, B. C.; Schadler, L. S.; Acehan, D.; Panagiotopoulos, A. Z.; Pryamitsyn, V.; et al. Anisotropic Self-Assembly of Spherical Polymer-Grafted Nanoparticles. *Nat. Mater.* **2009**, *8*, 354–359.
24. Islam, M. F.; Rojas, E.; Bergey, D. M.; Johnson, A. T.; Yodh, A. G. High Weight Fraction Surfactant Solubilization of Single-Wall Carbon Nanotubes in Water. *Nano Lett.* **2003**, *3*, 269–273.
25. Bryning, M. B.; Milkie, D. E.; Islam, M. F.; Hough, L. A.; Kikkawa, J. M.; Yodh, A. G. Carbon Nanotube Aerogels. *Adv. Mater.* **2007**, *19*, 661–664.
26. Hough, L. A.; Islam, M. F.; Hammouda, B.; Yodh, A. G.; Heiney, P. A. Structure of Semidilute Single-Wall Carbon Nanotube Suspensions and Gels. *Nano Lett.* **2006**, *6*, 313–317.
27. Hough, L. A.; Islam, M. F.; Janmey, P. A.; Yodh, A. G. Viscoelasticity of Single Wall Carbon Nanotube Suspensions. *Phys. Rev. Lett.* **2004**, *93*, 168102.
28. Kim, K. H.; Oh, Y.; Islam, M. F. Graphene Coating Makes Carbon Nanotube Aerogels Superelastic and Resistant to Fatigue. *Nat. Nanotechnol.* **2012**, *7*, 562–566.
29. Kim, K. H.; Oh, Y.; Islam, M. F. Mechanical and Thermal Management Characteristics of Ultrahigh Surface Area Single-Walled Carbon Nanotube Aerogel. *Adv. Funct. Mater.* **2013**, *23*, 377–383.
30. Kim, K. H.; Vural, M.; Islam, M. F. Single-Walled Carbon Nanotube Aerogel-Based Elastic Conductors. *Adv. Mater.* **2011**, *23*, 2865–2869.
31. Liff, S. M.; Kumar, N.; McKinley, G. H. High-Performance Elastomeric Nanocomposites *via* Solvent-Exchange Processing. *Nat. Mater.* **2007**, *6*, 76–83.
32. Xia, H.; Song, M. Preparation and Characterization of Polyurethane–Carbon Nanotube Composites. *Soft Matter* **2005**, *1*, 386–394.
33. Shin, M. K.; Oh, J.; Lima, M.; Kozlov, M. E.; Kim, S. J.; Baughman, R. H. Elastomeric Conductive Composites Based on Carbon Nanotube Forests. *Adv. Mater.* **2010**, *22*, 2663–2667.
34. Bansal, A.; Yang, H.; Li, C.; Cho, K.; Benicewicz, B. C.; Kumar, S. K.; Schadler, L. S. Quantitative Equivalence between Polymer Nanocomposites and Thin Polymer Films. *Nat. Mater.* **2005**, *4*, 693–698.
35. Oh, H.; Green, P. F. Polymer Chain Dynamics and Glass Transition in Athermal Polymer/Nanoparticle Mixtures. *Nat. Mater.* **2009**, *8*, 139–143.
36. Holt, B. D.; Short, P. A.; Rape, A. D.; Wang, Y.; Islam, M. F.; Dahl, K. N. Carbon Nanotubes Reorganize Actin Structures in Cells and *ex Vivo*. *ACS Nano* **2010**, *4*, 4872–4878.
37. Islam, M. F.; Milkie, D. E.; Torrens, O. N.; Yodh, A. G.; Kikkawa, J. M. Magnetic Heterogeneity and Alignment of Single Wall Carbon Nanotubes. *Phys. Rev. B* **2005**, *71*, 201401.
38. Gibson, R. F. *Principles of Composite Material Mechanics*; McGraw-Hill: New York, 1994.